PHILOSOPHICAL TRANSACTIONS A

rsta.royalsocietypublishing.org

Review

Cite this article: Balakireva IV, Chembo YK. 2018 A taxonomy of optical dissipative structures in whispering-gallery mode resonators with Kerr nonlinearity. *Phil. Trans. R. Soc. A* **376**: 20170381.
http://dx.doi.org/10.1098/rsta.2017.0381

Accepted: 17 March 2018

One contribution of 11 to a theme issue 'Dissipative structures in matter out of equilibrium: from chemistry, photonics and biology (part 1)'.

Subject Areas:
optics, complexity, applied mathematics

Keywords:
whispering-gallery mode resonators, Kerr combs, dissipative optical patterns, nonlinear optics

Author for correspondence:
Yanne K. Chembo
e-mail: yanne.chembo@femto-st.fr

THE ROYAL SOCIETY PUBLISHING

A taxonomy of optical dissipative structures in whispering-gallery mode resonators with Kerr nonlinearity

Irina V. Balakireva[1] and Yanne K. Chembo[1,2]

[1]FEMTO-ST Institute, Univ. Bourgogne Franche-Comté, CNRS, Optics Department, 15B Avenue des Montboucons, 25030 Besançon cedex, France

[2]GeorgiaTech-CNRS Joint International Laboratory [UMI 2958], Atlanta Mirror Site, School of Electrical and Computer Engineering, 777 Atlantic Drive Northwest, Atlanta, GA 30332, USA

YKC, 0000-0002-8375-0020

In this paper, the research related to the formation of optical dissipative structures in Kerr-nonlinear whispering-gallery mode resonators pumped with continuous-wave lasers is reviewed. Pattern formation in these systems can be analysed using the paradigmatic Lugiato–Lefever model, which is a partial differential equation ruling the dynamics of the intra-cavity laser field. Various dissipative structures such as Turing rolls, solitons, breathers and spatio-temporal chaos can emerge in the resonator depending on the laser power and frequency. The bifurcation analysis enables a classification of these patterns, and also permits identification of their basins of attraction.

This article is part of the theme issue 'Dissipative structures in matter out of equilibrium: from chemistry, photonics and biology (part 1)'.

1. Introduction

The topic of dissipative patterns in nonlinear optical cavities has been a very fertile area of research in the years following the invention of the laser. A paradigmatic model in this area is the Lugiato–Lefever equation (LLE), introduced 30 years ago by Luigi Lugiato and René Lefever to investigate the nonlinear dynamics of laser fields confined in nonlinear, diffractive and dissipative optical cavities [1].

Indeed, nonlinear partial differential equations (PDEs) analogous to the LLE had been introduced earlier to investigate the complex behaviour of plasmas [2], one-dimensional condensates [3] and dissipative solitons [4]. The dispersive LLE was introduced later on by Haelterman, Trillo and Wabnitz in the context of fibre ring cavities [5]. A special issue devoted to the theory and applications of the LLE has been published recently and provides an excellent overview of the current research in that field [6].

From a broader perspective, the research related to the LLE is intimately related to the fundamental concepts pioneered by Ilya Prigogine about the formation of dissipative structures in complex dynamical systems [7,8].

In the context of nonlinear photonics, one of the most important innovations in recent years has been the introduction of ultrahigh-Q whispering-gallery mode (WGM) resonators as a novel platform to investigate the dynamical properties of optical dissipative patterns. Effectively, the long-lifetime intra-cavity photons can efficiently interact via the nonlinearities of the bulk medium [9,10]. For the particular case of the Kerr nonlinearity, the resonator enhances four-wave mixing interactions of the kind $\hbar\omega_a + \hbar\omega_b \rightarrow \hbar\omega_c + \hbar\omega_d$, where two input photons labelled a and b interact coherently via the Kerr nonlinearity to yield two output photons labelled c and d. Owing to this mechanism of cascaded photonic interactions, it is possible to excite as many as several hundred cavity modes while pumping only one, and thereby obtain a coherent optical frequency comb [11]. These optical frequency combs are generally referred to as Kerr combs in the scientific literature, and they are expected to provide major technological breakthroughs in modern photonics [12–14].

However, in order to fulfill the promise of a technological dividend, a prerequisite is to achieve a clear understanding of the spatio-temporal dissipative patterns leading to these Kerr combs. It was shown a few years ago that the LLE is an ideal model in this regard as it accounts for the five main effects that are in play, namely laser frequency, laser power, dispersion, losses and Kerr nonlinearity [15–19]. In this article, an overview of the main theoretical results obtained from the LLE analysis for Kerr comb generation is proposed. The structure of the article is as follows. In the next section, the LLE model in the context of Kerr-nonlinear WGM resonators is briefly presented. Section 3 analyses the existence and stability of stationary dissipative patterns, as well as the bifurcations among them. The case of non-stationary patterns is discussed in §4. The final section provides a conclusion.

2. System and model

Modelling optical dissipative patterns in WGM resonators must account for certain relevant parameters which are related to the geometry of the resonator, to the properties of its bulk material, and to the coupling conditions.

From the geometrical perspective, the WGM resonators are characterized by their main radius a, or more precisely, the perimeter $L = 2\pi a$, followed by an intra-cavity photon to perform one round trip. This radius defines the free spectral range (FSR) of the resonator as $F_{\mathrm{FSR}} = c/n_g L = v_g/L$, where c is the velocity of light in vacuum, n_g is the group-velocity refraction index at the pump wavelength and v_g is the corresponding group velocity. The resonators are always multimode, with a large number of radial, polar, polarization and azimuthal modes.

Each of them is unambiguously identified by a single eigenparameter [10,14]. However, in the simplest configurations, spatio-temporal patterns leading to Kerr combs only involve a single family of modes, that is, a set of modes having the same eigenparameters except for the azimuthal ones. These azimuthal modes have an integer wavenumber ℓ, which quantifies the angular momentum of the photons as $\hbar\ell/a$. If ℓ_0 is considered as the eigennumber of the pumped mode of frequency ω_0, the azimuthal modes of interest have a reduced eigennumber $l = \ell - \ell_0$ that symmetrically expand as $l = \pm 1, \pm 2, \ldots$ around the pump. The corresponding eigenfrequencies ω_l can be Taylor-expanded as $\omega_l = \omega_0 + \sum_{k=1}^{+\infty} (\zeta_k/k!) l^k$, with $\zeta_1 \equiv 2\pi F_{\mathrm{FSR}} = \Omega_{\mathrm{FSR}}$ being the FSR, ζ_2 the group-velocity dispersion (GVD), and ζ_k for $k \geq 3$ representing the higher-dispersion terms. The photons are confined in torus-like azimuthal modes with an effective mode volume

$V_{\mathrm{eff}} = LA_{\mathrm{eff}}$, with A_{eff} being the effective mode area. The resonances have a loaded quality factor $Q = \omega_0 \tau_{\mathrm{ph}}$, where τ_{ph} is the photon lifetime. Typically, $Q \sim 10^6$–10^9 at 1550 nm, and accordingly, τ_{ph} ranges from a few nanoseconds to a few microseconds. The corresponding half-linewidth for these resonances is $\kappa = \omega_0/2Q = \kappa_{\mathrm{in}} + \kappa_{\mathrm{ext}}$, which has intrinsic (bulk) and extrinsic (coupling) contributions. Finally, the nonlinear parameter of the system is the bulk Kerr nonlinearity, which modifies the refraction index as $n = n_0 + n_2 I$, where n_0 is the refraction index at the frequency ω_0, n_2 is the Kerr coefficient, and I is the irradiance of the laser field. When the power of intra-cavity fields is measured in watts, the relevant nonlinear parameter is $\gamma = \omega_0 n_2 / c A_{\mathrm{eff}}$ (in $\mathrm{W}^{-1}\,\mathrm{m}^{-1}$). The pump laser is characterized by its power P_{L} and its angular frequency ω_{L}, which are both the main control parameters of the system.

Using the parameters defined above, the generalized LLE ruling the dynamics of the intra-cavity field $\mathcal{E}(\theta, t)$ can then be explicitly written as a function of time t and of the azimuthal angle $\theta \in [-\pi, \pi]$ along the perimeter of the resonator, following:

$$\frac{\partial \mathcal{E}}{\partial t} = -\kappa \mathcal{E} + \mathrm{i}\sigma \mathcal{E} + \mathrm{i} v_{\mathrm{g}} \sum_{k=2}^{K} (\mathrm{i}\Omega_{\mathrm{FSR}})^k \frac{\beta_k}{k!} \frac{\partial^k \mathcal{E}}{\partial \theta^k} + \mathrm{i} v_{\mathrm{g}} \gamma |\mathcal{E}|^2 \mathcal{E} + \sqrt{\frac{2\kappa_{\mathrm{ext}}}{T_{\mathrm{FSR}}}} \sqrt{P_{\mathrm{L}}}, \tag{2.1}$$

where $\beta_k = -\zeta_k/(-\Omega_{\mathrm{FSR}})^k v_{\mathrm{g}}$ stands for the dispersion, and $\sigma = \omega_{\mathrm{L}} - \omega_0$ for the detuning between the laser and resonance frequencies. In the above equation, the group-velocity dynamics of the intra-cavity field (proportional to $\beta_1 \partial_\theta \mathcal{E}$) have been discarded, and the normalization is such that $|\mathcal{E}|^2$ is in units of watts.

By restricting to the case with no higher-order dispersion, the above equation can be suitably normalized as

$$\frac{\partial \psi}{\partial \tau} = -(1 + \mathrm{i}\alpha)\psi - \mathrm{i}\frac{\beta}{2} \frac{\partial^2 \psi}{\partial \theta^2} + \mathrm{i}|\psi|^2 \psi + F, \tag{2.2}$$

where $\psi \equiv (\gamma v_{\mathrm{g}}/\kappa)^{1/2} \mathcal{E}$ is the total intra-cavity field, $\tau = \kappa t$ is the dimensionless time, $\alpha = -\sigma/\kappa$ is the cavity detuning, $\beta = -\zeta_2/\kappa = \beta_2 v_{\mathrm{g}} \Omega_{\mathrm{FSR}}^2/\kappa$ is the GVD (defined as normal for $\beta > 0$ and anomalous for $\beta < 0$), and finally, $F^2 = (2\gamma v_{\mathrm{g}}/T_{\mathrm{FSR}})(\kappa_{\mathrm{ext}}/\kappa^3) P_{\mathrm{L}}$ is the dimensionless laser pump power [16,18].

The dimensionless model of equation (2.2) is a powerful tool to analyse the nonlinear dynamics of the optical dissipative patterns that can be sustained in the WGM cavity. It should be emphasized that unlike many spatially extended systems, the spatial coordinate θ here is genuinely periodic as it directly originates from the closed-path trajectory of the photons, which relates to the modal structure of the resonator. In the following sections, classifications of the stationary and non-stationary dissipative patterns that are solutions of the LLE are provided, with emphasis on their condition of existence, stability and bifurcation behaviour.

3. Stationary dissipative structures

The stationary dissipative patterns are mainly characterized by their time-independence. The simplest stationary solution is the equilibrium state ψ_{e}, which is obtained by setting all the derivatives of the LLE to zero, following $F^2 = [1 + (\rho - \alpha)^2]\rho \equiv G(\alpha, \rho)$, with $\rho \equiv |\psi_{\mathrm{e}}|^2$. This cubic polynomial equation has one to three real-valued solutions in ρ depending on the parameters α and F. It can be shown that in the α–F^2 plane, the area corresponding to $\alpha > \sqrt{3}$ and $F^2 \in]F_-^2(\alpha), F_+^2(\alpha)[$ with

$$F_\pm^2(\alpha) = \frac{2\alpha \mp \sqrt{\alpha^2 - 3}}{3} \left[1 + \left(\frac{\sqrt{\alpha^2 - 3} \pm \alpha}{3} \right)^2 \right], \tag{3.1}$$

is the region where the system has three solutions. As is usually the case for systems with cubic nonlinearity, this area also corresponds to the one where hysterisis phenomena are observed, with

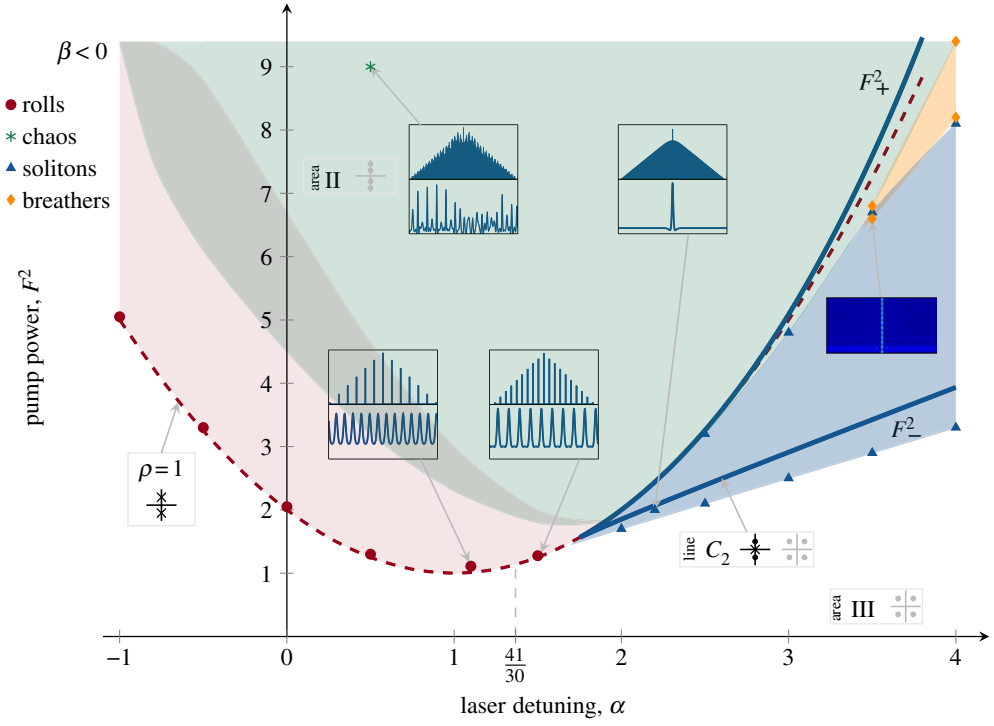

Figure 1. Bifurcation diagram for the anomalous dispersion regime ($\beta < 0$), as a function of the laser parameters α (frequency detuning) and F^2 (power). The inserts and pictograms have the same meaning as in figure 2. Blue solid lines correspond to $F^2_{\pm}$, while the red dashed line delineates $\rho = 1$. The blue area is the basin of attraction for bright solitons and soliton molecules. The pink area is the basin of attraction of Turing rolls. Breather solitons are obtained in the orange area. Spatio-temporal chaos is obtained in the green area. The buffer dark grey area between Turing rolls and spatio-temporal chaos is where secondary combs are observed. (Online version in colour.)

the two extremal solutions being stable while the intermediate solution is unstable. Outside this hysteresis area, there is only one equilibrium which is always asymptotically stable. The transition between the single- and triple-solution areas precisely occurs on the curves $F^2_{\pm}(\alpha)$, where there are two solutions. The solutions ψ_e are spatially uniform (θ-independent), and for that reason are often referred to as *flat states*.

The existence and stability of the stationary dissipative structures (which are time-independent but still θ-dependent) strongly depends on the spatial bifurcations from the flat states. The study of these spatial bifurcations permits identification of critical bifurcation boundaries that define the stability basins for the various patterns. This bifurcation study is performed by setting the temporal derivative to zero in equation (2.2), which is subsequently rewritten under the form of a four-dimensional spatial flow with the independent variables ψ, $\phi = \partial_\theta \psi$, ψ^* and $\phi^* = \partial_\theta \psi^*$.

The Jacobian of that flow around the flat states ψ_e explicitly reads

$$\mathbf{J} = \begin{bmatrix} 0 & 1 & 0 & 0 \\ \frac{2}{\beta}(2|\psi_e|^2 - \alpha + \mathrm{i}) & 0 & \frac{2}{\beta}\psi_e^2 & 0 \\ 0 & 0 & 0 & 1 \\ \frac{2}{\beta}\psi_e^{*2} & 0 & \frac{2}{\beta}(2|\psi_e|^2 - \alpha - \mathrm{i}) & 0 \end{bmatrix} \tag{3.2}$$

and the corresponding eigenvalues obey

$$\lambda^4 - \frac{4}{\beta}(2\rho - \alpha)\lambda^2 + \frac{4}{\beta^2}[1 - \rho^2 + (2\rho - \alpha)^2] = 0. \tag{3.3}$$

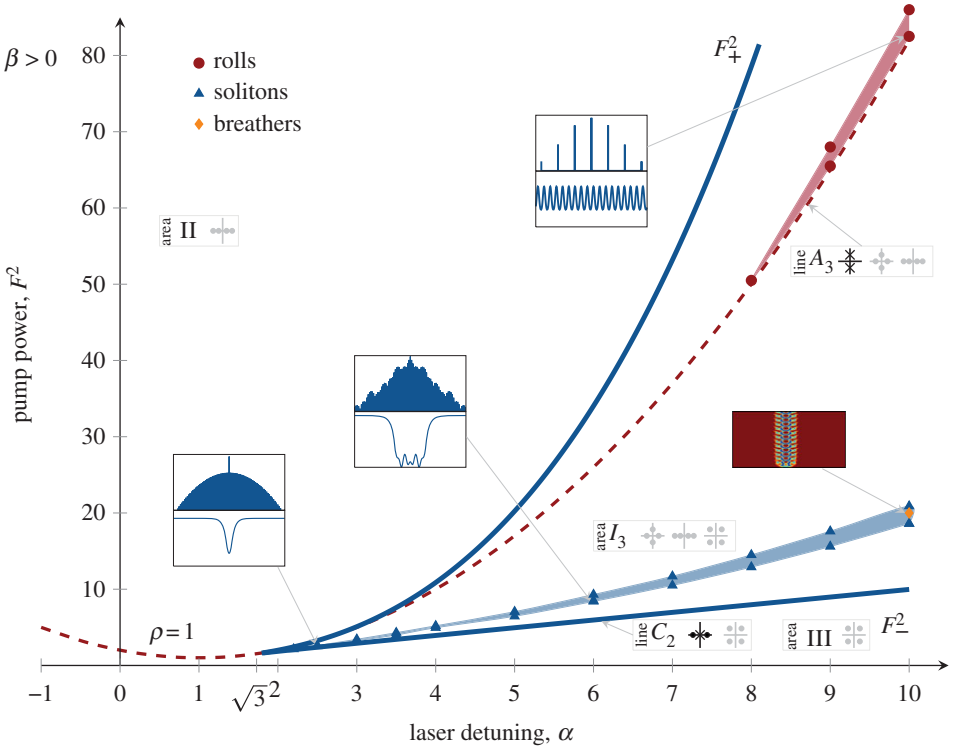

Figure 2. Bifurcation diagram for the normal dispersion regime ($\beta > 0$) as a function of the tunable laser parameters α (frequency detuning) and F^2 (power). In each insert, the top figure is a Kerr comb (frequency domain) while the bottom figure is the corresponding pattern (spatial domain $\theta \in [-\pi, \pi]$). The pictograms permit to analyse the various spatial bifurcations in the system. The blue solid lines correspond to $F^2_{\pm}$, and the red dashed line delineates $\rho = 1$. The blue area is the basin of attraction for dark solitons, platicons and breathers. The pink area is the basin of attraction of Turing rolls. (Online version in colour.)

The above equation is bi-quadratic and therefore yields for each equilibrium four eigenvalues which are either pairwise opposite when real-valued, or pairwise conjugated when complex-valued. Owing to the $\theta \to -\theta$ symmetry, the spatial bifurcations are *reversible*, and the bifurcations have an eigenvalue structure that is reminiscent of Hamiltonian systems. Analyzing the exact nature of these eigenvalues permits understanding of the topological changes of the intra-cavity field as a function of the laser pump frequency α and power F^2.

From the above analysis, it arises that the main bifurcation lines correspond to $F^2_{\pm}(\alpha)$ and to $F^2 = G(\alpha, 1)$ in the α–F^2 parametric plane. Both curves are represented in figures 1 and 2. In order to forecast a spatial bifurcation, the eigenvalue distribution has to be systematically evaluated along each of these lines. As explained in table 1, it is found that the system can sustain four types of bifurcations, namely quadruple-zero [or 0^4], Takens–Bogdanov [0^2], Takens–Bogdanov–Hopf [$0^2(\mathrm{i}\omega)$] and Hamiltonian–Hopf [$(\mathrm{i}\omega)^2$]. Some of these bifurcations are explicitly indicated in figures 1 and 2, where the pictograms in black are those highlighted in table 1, while those in grey correspond to the eigenvalue distributions that do not correspond to any spatial bifurcations. Regardless of the dispersion, it is found that no pattern can be created for low pump powers ($F^2 \to 0$), and the intra-cavity field remains a flat state in that case. However, there is always a threshold power beyond which stationary patterns emerge. The dynamical properties of these patterns appear to depend strongly on the dispersion regime.

In the anomalous dispersion case, dissipative patterns can always be generated above the Hamiltonian–Hopf bifurcation line $\rho = 1$, as can be seen in figure 1. When $\alpha < 2$, Turing rolls are generally obtained, which emerge via the modulational instability of the flat state. Indeed, this

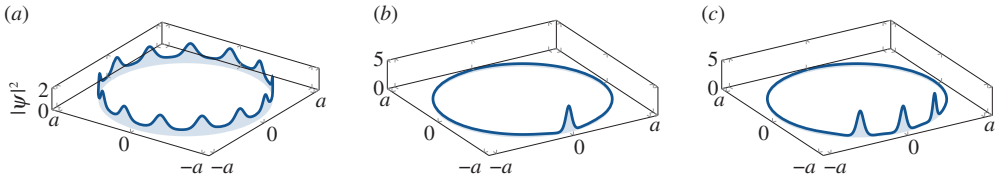

Figure 3. Stationary dissipative patterns in the anomalous dispersion regime ($\beta < 0$). (*a*) Rolls, (*b*) bright soliton and (*c*) soliton molecule. (Online version in colour.)

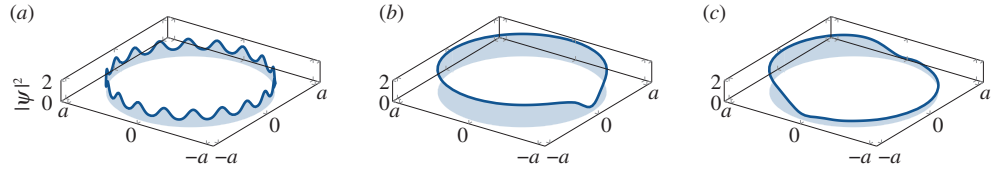

Figure 4. Stationary dissipative patterns in the normal dispersion regime ($\beta > 0$). (*a*) Rolls, (*b*) dark soliton and (*c*) platicon (or flaticon). (Online version in colour.)

Table 1. Pictograms for the various sets of eigenvalues. A set of four eigenvalues is attached to each equilibrium, and some classified bifurcations are attached to certain configurations of eigenvalues. A dot stands for one (simple) eigenvalue, the cross corresponds to a set of two degenerated eigenvalues and a circled cross stands for a set of four degenerated eigenvalues [18].

Eigenvalues and reversible spatial bifurcations in the Lugiato–Lefever model			
Nomenclature	Eigenvalues ($\lambda_{1,2}$; $\lambda_{3,4}$)	Pictogram	Bifurcation
Quadruple-zero	(0; 0)		0^4
Takens–Bogdanov	($\pm a$; 0)		0^2
Takens–Bogdanov–Hopf	(0; $\pm ib$)		$0^2(i\omega)$
Hamiltonian–Hopf	($\pm ia$; $\pm ia$)		$(i\omega)^2$

particular instability was first predicted by Alan Turing in his pioneering work on the chemical basis of morphogenesis [20]—the reason why this bifurcation is sometimes referred to as a *Turing bifurcation*. Roll patterns feature an integer number of maxima along the azimuthal direction, and correspondingly, the spectra are characterized by spectral lines spaced by the same integer number of FSRs. At threshold ($\rho = 1$), this number is the closest integer to $[2(\alpha - 2)/\beta]^{1/2}$. It was shown by Lugiato & Lefever in [1] that these rolls are super-critical when $\alpha < \frac{41}{30}$, and sub-critical otherwise. The stationary sub-critical patterns are essentially bright cavity solitons and soliton molecules, which correspond to bound solitons complexes. They should therefore not be confused with states where isolated solitons coexist in the cavity without mutual interaction (distance much greater than the soliton pulsewidth). The stationary patterns in the anomalous dispersion regime are displayed in figure 3. At the experimental level, numerous demonstrations of roll patterns (e.g. [21]) and solitons [22] have been reported in the literature.

In the normal dispersion case, dissipative patterns can only be generated in a very limited area of the parameter space. In fact, Turing rolls only arise marginally here, in a very narrow band just above the Hamiltonian–Hopf bifurcation when α is strongly detuned ($\gg 1$). As displayed in figure 4, there is another narrow band in the hysteresis area where solitonic solutions are

stable, and more precisely, dark solitons and platicons/flaticons [18,23]. These patterns have been experimentally demonstrated in [24].

4. Non-stationary dissipative structures

Depending on the pumping conditions, the dissipative patterns can become non-stationary and display an explicit time-dependence. Indeed, the temporal dynamics of the intra-cavity field will have the timescale of the photon lifetime, and will therefore be slow. These non-stationary patterns always arise after the stationary ones outlined in §3 lose their stability. They are therefore essentially unstable rolls or solitonic patterns.

Understanding how this loss of stability occurs requires perturbation of the spatially dependent solutions and monitoring of the asymptotic behaviour of the perturbation. A convenient way to achieve this procedure is to start with a modal decomposition of the intra-cavity field following $\psi(\theta,\tau)=\sum_l \Psi_l(\tau)\,\mathrm{e}^{\mathrm{i}l\theta}$, where $\Psi_l(\tau)$ is the time-varying amplitude of the mode of azimuthal order l. By plugging this expansion into the LLE, the following set of ordinary differential equations ruling the dynamics of each mode is obtained:

$$\dot{\Psi}_l=\left[-(1+\mathrm{i}\alpha)+\mathrm{i}\frac{\beta}{2}l^2\right]\Psi_l+\mathrm{i}\sum_{m,n,p}\delta(m-n+p-l)\Psi_m\Psi_n^*\Psi_p+\delta(l)F, \tag{4.1}$$

where the overdot denotes the derivative relatively to the dimensionless time τ, while m, n, p and l are azimuthal eigennumbers labelling the interacting modes following $\hbar\omega_m+\hbar\omega_p\rightarrow\hbar\omega_n+\hbar\omega_l$. Equation (4.1) corresponds to the modal expansion—or *spectro-temporal*—model that was initially proposed to investigate Kerr comb generation, before the spatio-temporal LLE model was demonstrated as equivalent [10,13,14].

The solutions corresponding to the stationary patterns are obtained by setting the temporal derivatives of the oscillating modes to zero in equation (4.1), following $\dot{\Psi}_l\equiv 0$. If a Kerr comb spanning from $l=-N$ to $l=N$ is considered, a set of $(2N+1)$ nonlinear, algebraic and coupled equations is thereby obtained. The perturbations around these steady-state solutions are obtained after differentiating equation (4.1) following:

$$\delta\dot{\Psi}_l=\sum_{p=-N}^{N}\mathcal{R}_{lp}\delta\Psi_p+\sum_{p=-N}^{N}\mathcal{S}_{lp}\delta\Psi_p^*, \tag{4.2}$$

where the complex-valued parameters

$$\mathcal{R}_{lp}=\left[-(1+\mathrm{i}\alpha)+\mathrm{i}\frac{\beta}{2}l^2\right]\delta(p-l)+2\mathrm{i}\sum_{m,n}\delta(m-n+p-l)\Psi_m\Psi_n^* \tag{4.3}$$

and

$$\mathcal{S}_{lp}=\mathrm{i}\sum_{m,n}\delta(m+n-p-l)\Psi_m\Psi_n, \tag{4.4}$$

can be considered as the elements of the $(2N+1)$th-order square matrices $\mathbf{R}$ and $\mathbf{S}$. If the $(2N+1)$-dimensional perturbation vector $\delta\Psi(\tau)=[\delta\Psi_{-N}(\tau),\ldots,\delta\Psi_N(\tau)]$ are introduced, then equation (4.2) can be written under the form of a flow:

$$\begin{bmatrix}\delta\dot{\Psi}\\ \delta\dot{\Psi}^*\end{bmatrix}=\mathbf{J}\begin{bmatrix}\delta\Psi\\ \delta\Psi^*\end{bmatrix},\quad\text{with }\mathbf{J}=\begin{bmatrix}\mathbf{R}&\mathbf{S}\\ \mathbf{S}^*&\mathbf{R}^*\end{bmatrix} \tag{4.5}$$

being a composite (block matrix) Jacobian of order $2(2N+1)$. Studying the asymptotic dynamics of the flow of equation (4.5) permits analysis of the stability of the stationary patterns, which are essentially rolls and cavity solitons. The result of this analysis is that the non-stationary dissipative patterns have dynamical features that are strongly correlated to those of the precursor stationary pattern.

On the one hand, localized stationary patterns such as cavity solitons generally undergo a Hopf bifurcation to morph into soliton breathers, which oscillate periodically in time at a

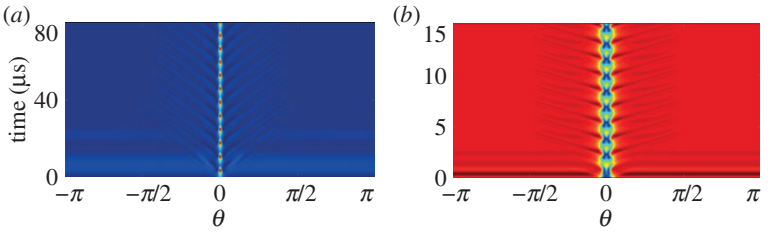

Figure 5. Spatio-temporal evolution of cavity soliton breathers, which are localized, non-stationary and periodic dissipative patterns. (*a*) Bright soliton breather in the anomalous dispersion regime. (*b*) Dark soliton breather in the normal dispersion regime. (Online version in colour.)

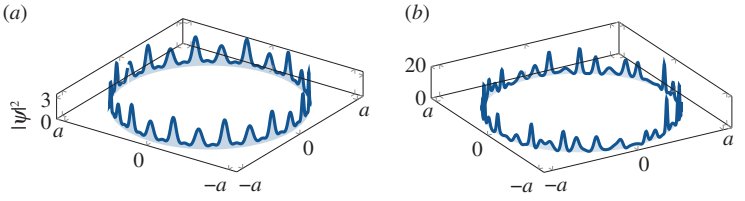

Figure 6. Extended non-stationary patterns in the anomalous dispersion regime. (*a*) Oscillating rolls and (*b*) spatio-temporal chaos. (Online version in colour.)

timescale comparable to the photon lifetime. As shown in figure 5, this behaviour is observed in both the anomalous and normal dispersion cases, leading to bright and dark soliton breathers. These oscillatory solitons have experimentally been evidenced in [25,26]. On the other hand, extended stationary patterns such as rolls lose their stability via a bifurcation that leads them to oscillate alternatively, as displayed in figure 6. In all cases, strong pumping leads to spatio-temporal chaos, and even eventually to rogue waves [10,13,14,27].

5. Conclusion

In this article, the optical dissipative structures that can emerge in a Kerr-nonlinear whispering-gallery mode resonator pumped with a resonant continuous-wave laser were briefly reviewed. The Lugiato–Lefever equation was used to investigate analytically the nature, stability and bifurcation behaviour of these patterns that could be localized or extended, stationary or non-stationary, and in the latter case, periodic or aperiodic. Interestingly, it has to be emphasized that the dynamical properties of the LLE are still under investigation from a purely mathematical point of view [28–31], and are continuously providing new insights with regards to the relationship between the LLE and other nonlinear PDEs [32]. Beyond the theoretical analysis, the dissipative patterns of WGM resonators are also enabling technology in several areas of photonics technology that would benefit from a better understanding of their properties [9,10,12–14,33–36]. The case here was considered where the WGM resonator has a Kerr nonlinearity and second-order dispersion. However, higher-order dispersion sometimes has to be accounted for and leads to new families of patterns [10,14,37]. It is well known that these cavities can also feature dissipative patterns induced by Raman [38,39] and Brillouin [40] nonlinearities, or even a combination of many of these effects [41,42]. The study of dissipative pattern formation in these cases is still embryonic, and will probably unveil new phenomenologies in the near future.

It is strongly believed that the dissipative patterns observed in nonlinear WGM resonators will continue to provide noteworthy contributions in relation to Ilya Prigogine's pioneering concepts of dissipative structures in complex dynamical systems.

Data accessibility. Data corresponding to the numerical simulations are available upon reasonable request to irina.balakireva@femto-st.fr or yanne.chembo@femto-st.fr.

Authors' contributions. I.V.B. performed the analytical study and the numerical simulations. Y.K.C. conceived and supervised the research project. Both authors wrote the article.

Competing interests. The authors declare that they have no competing interests.

Funding. This research has been funded by the ERC Project NextPhase (StG 278616).

Acknowledgements. The authors thank the *Mésocentre de calcul de Franche-Comté* for the computational resources.

References

1. Lugiato LA, Lefever R. 1987 Spatial dissipative structures in passive optical systems. *Phys. Rev. Lett.* **58**, 2209–2212. (doi:10.1103/PhysRevLett.58.2209)
2. Morales GJ, Lee YC. 1974 Ponderomotive-force effects in a nonuniform plasma. *Phys. Rev. Lett.* **33**, 1016–1019. (doi:10.1103/PhysRevLett.33.1016)
3. Kaup DJ, Newell AC. 1978 Theory of nonlinear oscillating dipolar excitations in one-dimensional condensates. *Phys. Rev. B* **18**, 5162–5167. (doi:10.1103/PhysRevB.18.5162)
4. Nozaki K, Bekki N. 1984 Solitons as attractors of a forced dissipative nonlinear Schrödinger equation. *Phys. Lett. A* **102**, 383–386. (doi:10.1016/0375-9601(84)91060-0)
5. Haelterman M, Trillo S, Wabnitz S. 1992 Dissipative modulation instability in a nonlinear dispersive ring cavity. *Opt. Commun.* **91**, 401–407. (doi:10.1016/0030-4018(92)90367-Z)
6. Chembo YK, Gomila D, Tlidi M, Menyuk CR. 2017 Theory and applications of the Lugiato–Lefever equation. *Eur. Phys. J. D* **71**, 299. (doi:10.1140/epjd/e2017-80572-0)
7. Prigogine I. 1967 Dissipative structures in chemical systems. In *Fast reactions and primary processes in chemical kinetics* (ed. S Claesson), pp. 371–382. New York, NY: Interscience.
8. Prigogine I, Lefever R. 1968 Symmetry breaking instabilities in dissipative systems. II. *J. Chem. Phys.* **48**, 1695–1700. (doi:10.1063/1.1668896)
9. Strekalov DV, Marquardt C, Matsko AB, Schwefel HG, Leuchs G. 2016 Nonlinear and quantum optics with whispering gallery resonators. *J. Opt.* **18**, 123002. (doi:10.1088/2040-8978/18/12/123002)
10. Lin G, Coillet A, Chembo YK. 2017 Nonlinear photonics with high-Q whispering-gallery-mode resonators. *Adv. Opt. Photonics* **9**, 828–890. (doi:10.1364/AOP.9.000828)
11. Del'Haye P, Schliesser A, Arcizet A, Holzwarth R, Kippenberg TJ. 2007 Optical frequency comb generation from a monolithic microresonator. *Nature* **450**, 1214–1217. (doi:10.1038/nature06401)
12. Kippenberg TJ, Holzwarth R, Diddams SA. 2011 Microresonator-based optical frequency combs. *Science* **322**, 555–559. (doi:10.1126/science.1193968)
13. Chembo YK. 2016 Kerr optical frequency combs: theory, applications and perspectives. *Nanophotonics* **5**, 214–230. (doi:10.1515/nanoph-2016-0013)
14. Pasquazi A *et al.* 2018 Micro-combs: a novel generation of optical sources. *Phys. Rep.* **729**, 1–81. (doi:10.1016/j.physrep.2017.08.004)
15. Matsko AB, Savchenkov AA, Liang W, Ilchenko VS, Seidel D, Maleki L. 2011 Mode-locked Kerr frequency combs. *Opt. Lett.* **36**, 2845–2847. (doi:10.1364/OL.36.002845)
16. Chembo YK, Menyuk CR. 2013 Spatiotemporal Lugiato–Lefever formalism for Kerr-comb generation in whispering-gallery-mode resonators. *Phys. Rev. A* **87**, 053852. (doi:10.1103/PhysRevA.87.053852)
17. Coen S, Randle HG, Sylvestre T, Erkintalo M. 2013 Modeling of octave-spanning Kerr frequency combs using a generalized mean-field Lugiato–Lefever model. *Opt. Lett.* **38**, 37–39. (doi:10.1364/OL.38.000037)
18. Godey C, Balakireva IV, Coillet A, Chembo YK. 2014 Stability analysis of the spatiotemporal Lugiato–Lefever model for Kerr optical frequency combs in the anomalous and normal dispersion regimes. *Phys. Rev. A* **89**, 063814. (doi:10.1103/PhysRevA.89.063814)
19. Parra-Rivas P, Gomila D, Matias MA, Coen S, Gelens L. 2014 Dynamics of localized and patterned structures in the Lugiato–Lefever equation determine the stability and shape of optical frequency combs. *Phys. Rev. A* **89**, 043813. (doi:10.1103/PhysRevA.89.043813)
20. Turing AM. 1952 The chemical basis of morphogenesis. *Phil. Trans. R. Soc. Lond. B* **237**, 37–72. (doi:10.1098/rstb.1952.0012)
21. Pfeifle J *et al.* 2015 Optimally coherent Kerr combs generated with crystalline whispering gallery mode resonators for ultrahigh capacity fiber communications. *Phys. Rev. Lett.* **114**, 093902. (doi:10.1103/PhysRevLett.114.093902)

22. Herr T, Brasch V, Jost JD, Wang CY, Kondratiev NM, Gorodetsky ML, Kippenberg TJ. 2014 Temporal solitons in optical microresonators. *Nat. Photonics* **8**, 145–152. (doi:10.1038/nphoton.2013.343)
23. Lobanov VE, Lihachev G, Kippenberg TJ, Gorodetsky ML. 2015 Frequency combs and platicons in optical microresonators with normal GVD. *Opt. Express* **23**, 7713–7721. (doi:10.1364/OE.23.007713)
24. Xue X, Xuan Y, Liu Y, Wang PH, Chen S, Wang J, Leaird DE, Qi M, Weiner AM. 2015 Mode-locked dark pulse Kerr combs in normal-dispersion microresonators. *Nat. Photonics* **9**, 594–600. (doi:10.1038/nphoton.2015.137)
25. Bao C, Jaramillo-Villegas JA, Xuan Y, Leaird DE, Qi M, Weiner AM. 2016 Observation of Fermi-Pasta-Ulam recurrence induced by breather solitons in an optical microresonator. *Phys. Rev. Lett.* **117**, 163901. (doi:10.1103/PhysRevLett.117.163901)
26. Yu M, Jang JK, Okawachi Y, Griffith AG, Luke K, Miller SA, Ji X, Lipson M, Gaeta AL. 2017 Breather soliton dynamics in microresonators. *Nat. Commun.* **8**, 14569. (doi:10.1038/ncomms14569)
27. Liu Z, Ouali M, Coulibaly S, Clerc MG, Taki M, Tlidi M. 2017 Characterization of spatiotemporal chaos in a Kerr optical frequency comb and in all fiber cavities. *Opt. Lett.* **42**, 1063–1066. (doi:10.1364/OL.42.001063)
28. Miyaji T, Ohnishi I, Tsutsumi Y. 2010 Bifurcation analysis to the Lugiato–Lefever equation in one space dimension. *Phys. D* **239**, 2066–2083. (doi:10.1016/j.physd.2010.07.014)
29. Kozyreff G. 2012 Localized turing patterns in nonlinear optical cavities. *Phys. D* **241**, 936–946. (doi:10.1016/j.physd.2012.02.007)
30. Godey C. 2017 A bifurcation analysis for the Lugiato–Lefever equation. *Eur. Phys. J. D* **71**, 131. (doi:10.1140/epjd/e2017-80057-2)
31. Mandel R, Reichel W. 2017 A priori bounds and global bifurcation results for frequency combs modeled by the Lugiato–Lefever equation. *SIAM J. Appl. Math.* **77**, 315–345. (doi:10.1137/16M1066221)
32. Ferré MA, Clerc MG, Coulibally S, Rojas RG, Tlidi M. 2017 Localized structures and spatiotemporal chaos: comparison between the driven damped sine-Gordon and the Lugiato–Lefever model. *Eur. Phys. J. D* **71**, 172. (doi:10.1140/epjd/e2017-80072-3)
33. Coillet A, Henriet R, Huy KP, Jacquot M, Furfaro L, Balakireva I, Larger L, Chembo YK. 2013 Microwave photonics systems based on whispering-gallery-mode resonators. *J. Vis. Exp.* **78**, e50423. (doi:10.3791/50423)
34. Liang W, Eliyahu D, Ilchenko VS, Savchenkov AA, Matsko AB, Seidel D, Maleki L. 2015 High spectral purity Kerr frequency comb radio frequency photonic oscillator. *Nat. Commun.* **6**, 7957. (doi:10.1038/ncomms8957)
35. Saleh K, Chembo YK. 2016 On the phase noise performance of microwave and millimeter-wave signals generated with versatile Kerr optical frequency combs. *Opt. Express* **24**, 25 043–25 056. (doi:10.1364/OE.24.025043)
36. Saleh K, Henriet R, Diallo S, Lin G, Martinenghi R, Balakireva IV, Salzenstein P, Coillet A, Chembo YK. 2014 Phase noise performance comparison between optoelectronic oscillators based on optical delay lines and whispering gallery mode resonators. *Opt. Express* **22**, 32 158–32 173. (doi:10.1364/OE.22.032158)
37. Milián C, Skryabin DV. 2014 Soliton families and resonant radiation in a micro-ring resonator near zero group-velocity dispersion. *Opt. Express* **22**, 3732–3739. (doi:10.1364/OE.22.003732)
38. Lin G, Chembo YK. 2016 Phase-locking transition in Raman combs generated with whispering gallery mode resonators. *Opt. Lett.* **41**, 3718–3721. (doi:10.1364/OL.41.003718)
39. Yang QF, Yi X, Yang KY, Vahala K. 2016 Stokes solitons in optical microcavities. *Nat. Phys.* **13**, 53–57. (doi:10.1038/nphys3875)
40. Diallo S, Lin G, Martinenghi R, Furfaro L, Jacquot M, Chembo YK. 2016 Brillouin lasing in ultra-high-q lithium fluoride disk resonators. *IEEE Photonics Tech. Lett.* **28**, 955–958. (doi:10.1109/LPT.2016.2521341)
41. Chembo YK, Grudinin IS, Yu N. 2015 Spatiotemporal dynamics of Kerr-Raman optical frequency combs. *Phys. Rev. A* **92**, 043818. (doi:10.1103/PhysRevA.92.043818)
42. Lin G, Diallo S, Dudley JM, Chembo YK. 2016 Universal nonlinear scattering in ultra-high Q whispering gallery-mode resonators. *Opt. Express* **24**, 14 880–14 894. (doi:10.1364/OE.24.014880)